Survey on Vertical Two-Phase Countercurrent Flooding

EPRI

Keywords:
Countercurrent
Flooding
Wave
Instability
Interfacial
LOCA

EPRI NP-984
Project 1160-1
Topical Report
February 1979

Prepared by
University of California
Berkeley, California

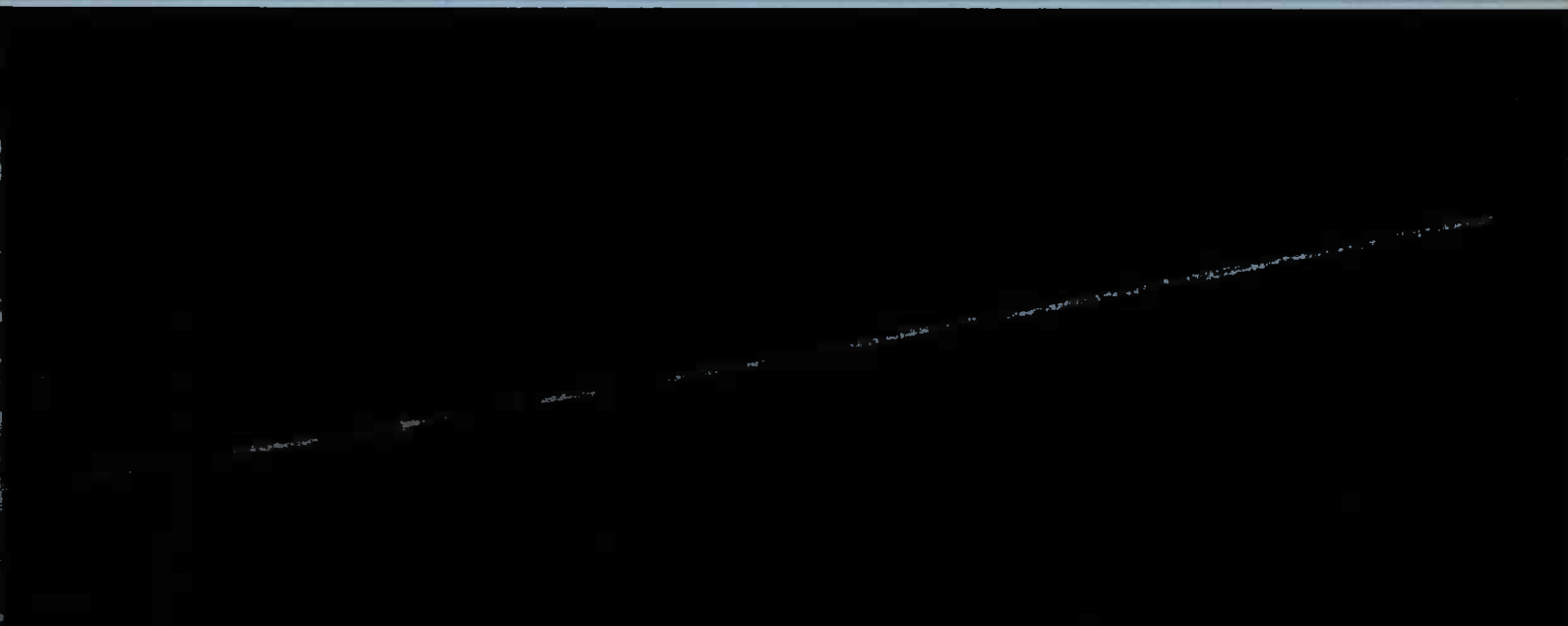

ELECTRIC POWER RESEARCH INSTITUTE

Survey on Vertical Two-Phase Countercurrent Flooding

NP-984
Research Project 1160-1

Topical Report, February 1979

Prepared by

UNIVERSITY OF CALIFORNIA
Department of Mechanical Engineering
Berkeley, California 94720

Principal Investigators
C. L. Tien
C. P. Liu

Prepared for

Electric Power Research Institute
3412 Hillview Avenue
Palo Alto, California 94304

EPRI Project Manager
K. H. Sun
Nuclear Power Division

ORDERING INFORMATION

Requests for copies of this report should be directed to Research Reports Center (RRC), Box 10090, Palo Alto, CA 94303, (415) 961-9043. There is no charge for reports requested by EPRI member utilities and affiliates, contributing nonmembers, U.S. utility associations, U.S. government agencies (federal, state, and local), media, and foreign organizations with which EPRI has an information exchange agreement. On request, RRC will send a catalog of EPRI reports.

NOTICE

Prepared by
University of California
Berkeley, California

EPRI PERSPECTIVE

PROJECT DESCRIPTION

For the hypothetical loss-of-coolant accident in a light water reactor (LWR), rapid reflooding of the core region is essential. Thus the emergency core-cooling systems provide a large amount of water to reflood the core. Along the coolant passage, however, the downward flow of coolant water may be limited by the upward flow of steam generated by water evaporation in the core and lower plenum. This limiting phenomenon is generally known as countercurrent flooding. The most widely used semiempirical flooding correlations in current LWR evaluation models are those of Wallis and of Kutateladze.

The Wallis and the Kutateladze correlations are similar in several aspects; in particular, the similar functional expression and the absence of viscosity in the correlations. However, there do exist some fundamental differences; namely, the characteristic-length parameter in the Wallis correlation and the presence of surface tension in the Kutateladze correlation. These differences lead to a different scaling basis for the countercurrent flooding phenomenon. This project of analytical and experimental studies will help clarify the scaling uncertainties in the current LWR evaluation models.

PROJECT OBJECTIVE

The project objective is to critically assess existing countercurrent flooding models, with particular emphasis on the validity and the limitations of the Wallis and the Kutateladze correlations. Flooding experiments will be performed for air-liquid countercurrent flows in a single, circular channel. Various liquids and tube diameters will be used to ascertain the effects of tube size, surface tension, and viscosity. The analytical basis of the flooding correlation will also be evaluated.

CONCLUSIONS AND RECOMMENDATIONS

This report documents the state-of-the-art review of the countercurrent flooding phenomenon in vertical two-phase flow. The survey covered 56 pertinent works

published since 1939. Various correlations for single-tube geometry are summarized in a table along with the information of the experimental tube sizes, the liquid inlet and exit configurations, and the testing fluids. The report should be valuable to those who use flooding correlations for design applications, and to researchers and engineers who are interested in two-phase flow.

K. H. Sun, Project Manager
Nuclear Power Division

TABLE OF CONTENTS

SUMMARY

This report reviews the available analytical developments and experimental studies on countercurrent flooding. Analytical modeling is still in its infancy. This may be attributed to the highly unsteady and chaotic nature of flooding, which greatly complicates mathematical treatment. Idealization and simplification were often introduced to make analysis possible. Despite its shortcomings, such analytical modeling does shed light on the basic mechanics of this phenomenon. Experimental studies have yielded many valuable results concerning various flooding parameters. A large number of correlations have been published. The most promising ones are the Wallis and Kutateladze correlations. Their formulations are similar; however, fundamental differences exist: the geometric-length parameter in the former correlation and the presence of a surface tension parameter in the latter. These differences lead to different scaling bases for the flooding pheonomenon and could lead to significant uncertainties for application to reactor LOCA analysis. While large-scale experiments are being conducted to study scaling, testing with different fluid properties, such as surface tension and viscosity, are gaining attention in the current flooding investigations.

Further efforts are needed for improving the analytical modeling of this phenomenon. More experimental data are required to clarify parametric dependencies, especially those of surface tension and viscosity. Additional work, both analytical and experimental, needs to be done on vapor condensation effects, liquid entrainment and multichannel flooding to improve the existing correlations and models.

1.0 INTRODUCTION

The flooding phenomenon in vertical counter-current two-phase flow systems first received attention from chemical engineers in the design of packed columns (1,2). In recent years, with the advent of nuclear technology and a growing interest in various heat transfer phenomena in two-phase flows, mechanical and nuclear engineers became also involved in the investigation of this phenomenon (3,4).

In the present review, the main interest in the flooding phenomenon concerns the potential limitation on the reflood process of the nuclear reactor core during a hypothetical loss-of-coolant accident (LOCA) of a pressurized water reactor (PWR) or a boiling water reactor (BWR) (5,6). In case of such an accident, the emergency core cooling systems (ECCS) reflood the reactor core with a coolant through either top spraying or bottom reflooding. However, along the coolant passage, the flow of the coolant may be limited by uprising steam generated from water-evaporation, such as in the BWR counter-current flow limit, the PWR upper head injection, and the PWR ECC by-pass. Therefore, a clear understanding of the flooding phenomenon becomes necessary for assessing the performance of these safety systems.

1.1 Physical Description of Flooding Phenomena

In a vertical two-phase counter-current flow situation, there is a limiting condition under which the flow rates of both phases cannot be increased further. This limiting condition is usually, especially in chemical engineering, referred to as "flooding" (5,7). For annular flows, this condition is marked by a highly unsteady and chaotic flow behavior (8). Some researchers adopted the criterion of zero liquid penetration (9) for flooding, others suggested the beginning of liquid flow reversal (10) while still others took the inception of liquid entrainment as their experimental criterion for the onset of flooding (11).

Based on visual observations on vertical counter-current flows, as the upward gas velocity increases under a constant liquid flow rate, the interface between the gas and liquid phase will become wavy. With increasing gas velocity, very large

wave formations appear on the interface, usually accompanied by a large pressure drop across the tube, and the gas flow rate reaches a limiting value. A further increase in gas velocity brings the onset of zero liquid penetration, followed by a complete liquid flow reversal, and the flow becomes co-current. When the liquid flow rate is slowly increased for a given gas velocity, a similar flooding phenomenon also occurs at a certain critical liquid flow rate. According to Wallis (12), the relationship between the gas and liquid flow rates in these two phenomena is not usually identical. However, most investigators did not make this distinction in their studies.

The exact physical mechanism of flooding remains undetermined. The existing physical models of flooding are mostly based on a consideration of interfacial instabilities (13-16). These instabilities are believed to cause liquid droplet entrainment and the bridging and churning of the liquid flow, characteristics often used as the flooding criterion in experiments. Because of the varied physical models and mathematical formulations, the lack of a standard criterion for the onset of flooding and the often conflicting experimental observations, there has been considerable controversy over existing analytical and experimental studies. In the absence of a satisfactory analytical understanding, the prediction of critical velocities at the onset of flooding is largely based on empirical correlations. However, these correlations were formulated from experimental data of a limited number of fluids and channel geometries, and the use of differring fluids or geometries often necessitates modifications of these correlations.

1.2 Scope of the Present Review

The present review consists of five sections. In Section 1, a brief introduction including a physical description of flooding in a counter-current flow is given. Section 2 reviews the existing analytical models which lead to the prediction of critical velocities at the onset of flooding in a single vertical channel. These models are based on the theory of hydrodynamics of a falling film under adiabatic conditions, and do not include the effects of heat transfer. Section 3 summarizes the experimental studies on single channel flooding and the published flooding correlations. The parametric dependence of these correlations is discussed. Section 4 examines extended problems in flooding: vapor condensation, liquid entrainment, inclined flows and flooding in simulated PWR and BWR geometries. Section 5 contains a summary of the present survey.

2.0 ANALYTICAL MODELING

Similar to many other complex flow situations, the exact mathematical treatment for the vertical two-phase counter-current flow is formidable. Extensive idealizations are required to simplify the governing equations in order to obtain any solution, either numerically or analytically. Existing analytical models are based on either the limiting case of a hanging film, also referred to as the case of zero penetration depth, or a small disturbance in the falling film, which is then treated by invicid or viscous flow theory.

2.1 Hanging Film Model

Grolmes et al. (17) assumed that, for a thin falling film, the Navier-Stoke equations can be reduced to one component along the axial direction,

$$\mu_f \frac{\partial^2 V_f}{\partial y^2} + \rho_f g = 0 \qquad (1)$$

with boundary conditions:

$$V_f = 0 \quad \text{at} \quad y = 0 \quad \text{(no slip at the wall)}$$

and

$$\mu_f \frac{\partial V_f}{\partial y} = \tau_i \quad \text{at} \quad y = \delta$$

where $\tau_i = \rho_g V_g^2 f_{2\phi}/2$ is the interface friction factor at the flooding transition, and δ is the Nusselt film thickness. Equation (1) can be integrated directly with the two boundary conditions to solve for V_f. The criterion for flooding is defined to be zero average liquid velocity, where the average velocity is expressed as

$$\langle V_f \rangle = \frac{1}{\delta} \int_0^{\delta} V_f dy$$

This leads to the result for the critical gas velocity as follows:

$$V_g = \frac{2}{\sqrt{3}} \left(\frac{\rho_f}{\rho_g}\right)^{\frac{1}{2}} \left(\frac{g\delta}{f_{2\phi}}\right)^{\frac{1}{2}} \quad . \tag{2}$$

Equation (2) contains a friction coefficient $f_{2\phi}$ which is determined empirically through correlating experimental data. These authors collected values of $f_{2\phi}$ at various film thicknesses, including those obtained by Toblevich et al. (18) and proposed:

$$f_{2\phi} = 0.006 + \frac{200\delta^2}{(\mu/\mu_R)^{0.44}} \quad .$$

Another analysis on a hanging film (See Fig. 1a), using the potential flow theory, was presented by Wallis and Kuo (19). Considering Bernoulli's equation for the gas and liquid phase, and the interface boundary condition of pressure continuity, these authors obtained a relation

$$\frac{1}{2}\left[\frac{\rho_g V_g^2}{\sqrt{(\rho_f-\rho_g)g\sigma}}\right]\left(\frac{d\phi^*}{dx^*}\right)^2 + \left(\frac{d\phi^*}{dy^*}\right)^2 + \frac{\frac{d^2x^*}{dy^{*2}}}{\{1+(\frac{dx^*}{dy^*})^2\}^{3/2}} +$$

$$\frac{\left|\frac{dx^*}{dy^*}\right|}{r^*[1+(\frac{dx^*}{dy^*})^2]^{\frac{1}{2}}} - (x_o^* - x^*) = \text{constant} \tag{3}$$

where $x^* = x(\frac{\Delta\rho g}{\sigma})^{\frac{1}{2}}$, $y^* = y(\frac{\Delta\rho g}{\sigma})^{\frac{1}{2}}$, $\phi^* = \frac{\phi}{Vgo}(\frac{\Delta\rho g}{\sigma})^{\frac{1}{2}}$, and σ denotes surface tension. A key dimensionless group which emerges from eq. (3) is the Kutateladze number:

$$K_g = \rho_g^{\frac{1}{2}} V_g [(\rho_f - \rho_g)\, g\sigma]^{-\frac{1}{4}} \tag{4}$$

Equation (3) shows various limiting behaviors. Three cases were examined: (a) Large D* (Bond number), K = 0, $dx^*/dr^* \to 0$ as $r^* \to \infty$; (b) Finite D*, K = 0; and (c) Large D*, K ≠ 0, β(contact angle) = 90°.

Case (a) corresponds to an extensive sheet of liquid with a shape of interface which is uniform in the third dimension. This problem was solved by Bankoff (20), with the following result:

$$y^* = \ell n \sqrt{\frac{4}{x^{*2}} - 1} + \frac{2}{x^*} - 2\sqrt{1 - \frac{x^{*2}}{4}} \tag{5}$$

which describes the shape of a large sheet of a hanging film interface.

In Case (b), Eq. (3) was solved numerically for $V_g = 0$, $dx^*/dr^* \to 0$ as $r^* \to \infty$. A family of curves was generated by varying the initial surface slope at large r*. These results describe the spreading of liquid film over the mouth of a sharp edged hole in a horizontal surface.

In Case (c), with the assumption of a small curvature for large D*, the Kutateladze number can also be derived from Eq. (3) as

$$K_g^2 = 2\left\{x_o^* + \sin^3\beta\left(\frac{d^2x^*}{dy^{*2}}\right)_{x_o} - x^* - \frac{\dfrac{d^2x^*}{dy^{*2}}}{\left[1+\left(\frac{dx^*}{dy^*}\right)^2\right]^{3/2}}\right\}\left|\frac{dw^*}{dz^*}\right|^{-2} \tag{6}$$

where w* is the dimensionless complex velocity, $\frac{w}{Vgo}\left(\frac{\Delta\rho g}{\sigma}\right)^{\frac{1}{2}}$, potential and β is the contact angle. Approximating the flow by a uniform flow over a pair of sources located at (o,±a) with strength A, the analytical expressions for both $x^* = f_1(y^*, a^*, A^*)$, where $A^* = \frac{A}{Vgo}\left(\frac{\Delta\rho g}{\sigma}\right)^{\frac{1}{2}}$, and the dimensionless velocity square $(dw^*/dz^*)^2 = f_2(x^*, y^*, a^*, A^*)$ can be found. Both x* and $(dw^*/dz^*)^2$, along with Eq. (6), were then used to compute the value of K_g at each point along the flow. This iteration process stops when a value of A* and a set of a*'s giving a reasonable constant K_g value (within 10% of the mean value) are found. As A*, a measure of the size of liquid projection, increases above two, the deviations in K_g go above 10 percent. These deviations become progressively larger as A* takes on a higher value; this fact was interpreted as a symptom of interface instability. The maximum value of K_g was found to be 1.87. In

general, the critical K_g value so obtained would be expected to depend on β, the contact angle.

Experiments were performed for each case examined. The results were generally consistent, both qualitatively and quantitatively, with the theoretical calculations. However, Puskina and Sorokin (10) and Lovell (9) showed experimentally that the limiting K_g value is around 3.2. Further discussion on this point will be presented in Section 3.

Ueda and Suzuki (21) proposed a model for interaction between the large amplitude wave on the liquid film falling down a vertical rod and the upward gas stream at the onset of flooding (see Fig. 1b). Shape of the wave crest is assumed to be flat because the wave tip is continuously torn off by gas flow (entrainment), and the wave is assumed to be stationary. These authors postulated that at the onset of flooding, the force balances in both the horizontal and vertical directions occur on the wave. From these force balances, the relationship between the gas velocity V_g and the wave height Δh, where Δh can be determined from (A_{gl}/A_{g0}), at the onset of flooding can be deduced as

$$\left(\frac{\rho_g}{\rho_f}\,\frac{V_{gl}^2}{2g}\right)\left(\frac{\rho_g}{\sigma}\,\frac{V_{gl}^2}{2}\right)\left(\frac{A_{gl}}{A_{g0}}\right)^2\left[\left(\frac{A_{gl}}{A_{g0}}\right)^2 - 1\right] = \eta_c \qquad (7)$$

where η_c is the wave profile factor. The gas flooding velocity so predicted with η_c and Δh estimated from the experimental data compared well with the measured values. Equation (7) was also applied to flow inside a tube, the comparison was also good.

2.2 Instabilities in Falling Films

The interface instabilities between two fluids in a horizontal stratified flow have been studied extensively. The four types of instabilities which, singly or in combination, can lead to flow waviness or a change in flow pattern are the Kelvin-Helmholtz, the Rayleigh-Taylor, the Tollmien-Schlichting and the Bernard instabilities. A comprehensive discussion of these instabilities in liquid films is given by Ostrach and Koestel (22).

The Bernard instability is associated with the adverse density gradient occurring in the horizontal liquid film with bottom heating; it does not constitute a relevant mechanism for the vertical falling film. The Kelvin-Helmholtz and Rayleigh-Taylor instabilities arise from the potential flow theory consideration whereas the Tollmien-Schlichting instability is a solution to the Orr-Sommerfeld stability equation derived from the Navier-Stokes equation based on small perturbation approximation.

2.2.1 Standing Wave Model

Shearer and Davidson (13) gave one of the earliest analytical treatments of flooding in the vertical counter-current flow. These authors based their analysis on the theory of a standing wave (see Fig. 1c). By assuming a parabolic liquid velocity distribution and a constant gas pressure over the leeward part of the wave, together with an empirical gas pressure distribution over the windward surface of the wave, a differential equation for the film thickness t was found to be:

$$\sigma \frac{d^3t}{dx^3} + \frac{\pi \rho_g V_g^2}{2\ell}\left(1 + \frac{\pi t}{2\ell}\right)\frac{dt}{dx} + \rho_f g + \frac{6}{5}\frac{\rho_f Q^2}{t^3}\frac{dt}{dx} - \frac{3\mu Q}{t^3} = 0 \qquad (8)$$

with boundary conditions at $x = 0$

$$t = a + t_0 , \quad dt/dx = 0$$

and $$(d^2t/dx^2)_{x=0} = -\left[\frac{3}{2} a(\rho_f g/\sigma)^2\right]^{1/3} \quad \text{(pressure continuity)}$$

where a is the wave amplitude and Q is the total flow rate in the liquid film. Equation (8) was solved by numerical integration based on Taylor's series expansion. From the solution obtained, it was concluded that the wave is only stable in a narrow range of gas flow rates. With minor modifications, the standing wave theory was applied to flooding in tubes. A comparison between the experimental results by Nicklin and Davidson (23) and other investigators (8,24) showed fairly good agreement up to the liquid Reynolds number of 1000. For $Re_f (= \frac{4\rho_f Q_f}{\mu})$ greater than 1000, large discrepancies were observed which Shearer and Davidson attributed to the onset of turbulence in the film flow. Later Clift et al. (25) showed that this analysis failed to give good agreement with experimental data for liquids of high viscosity.

2.2.2 The Orr-Sommerfeld Equation

A second theoretical approach to the flooding problem based on a linearized small-perturbation stability analysis was given by Cetinbudaklar and Jameson (14). Figure 2a shows the coordinate system on which this analysis was based. Assuming a sinusoidal interface disturbance, $\eta = a \exp(ik(x-ct))$, where c is the complex wave velocity,

$$c = c_r + ic_i$$

the Orr-Sommerfeld equation for the vertical film flow of thickness h depicted in Fig. 2a was obtained as

$$F'''' - 2k^2F'' + k^4F = ikRe_f[V_f^* - c)(F'' - k^2F) - V_f^{*\prime\prime} F] \qquad (9)$$

where $V_f^* = y^2=1$, a nondimensional velocity distribution, $Re = \frac{\rho V_{fo} h}{\mu}$ and F is related to the stream function by $\psi_f = -F(y)\eta$. Also (') denotes differentiation with respect to y and (0) denotes value at interface.

The boundary conditions are at the wall (y = -1),

$$F(-1) = F'(-1) = 0$$

and at the interface (y = 0),

$$F'(0) = c-V_{fo}^*$$

$$F''(0) = Ts - k^2(c-V_{fo}^*) - V_{fo}^{*\prime\prime} \qquad \text{(tangential stress continuity)}$$

$$(c-V_{fo}^*)F'(o) - \frac{i}{kRe}(F'''(o) - 3k^2F'(o)) = k^2We - k\frac{Ps}{Re} \text{ (normal stress continuity)}$$

where $We = \frac{\sigma}{\rho_f V_{fo}^2 h}$ the Weber number, and Ts and Ps are dimensionless stresses to be determined from a gas phase analysis which involves solving the truncated Orr-Sommerfeld equation for the gas flow

$$f^{iv} - \frac{i\rho_g k}{\mu_g}(V'_{go}\, y - c)\, f'' = 0 \qquad (10)$$

where V'_{go} is the velocity gradient in the gas phase at y = 0.

By arguing that the stability of the film is largely dependent on conditions near the interface where $V_f^{*'}$ is zero, then $V_f^* = V_{fo}^*$ = constant and $V_f'' = 2$, and Eq. (9) reduces to a fourth-order ordinary differential equation with constant coefficients, which has a closed-form analytical solution. This solution of F was then substituted into the four boundary conditions to solve for c_i and V_*, given k and Re with c_r set equal to V_{fo}^*, where V_* is the gas friction velocity defined as the square root of the ratio of the mean interfacial shear and the gas viscosity. The flooding velocity was taken to be the minimum V_* in the curve. Comparison of these results with the experimental data from Clift et al. (25) showed fairly good agreement. It was not possible to generate a single flooding correlation from this analysis, a major drawback of both this and Shear and Davidson's analysis.

It should be noted that the experimental study of a free falling water film down a vertical tube by Jones and Whitaker (26) showed that the numerical solution of the Orr-Sommerfeld equation is in good agreement with the experimental results near the top of the film where the small-disturbance assumption is expected to be valid.

2.2.3 Potential Flow Model

Kutateladze (27) argued that for the vanishingly small viscosity situation, the stability of the two-phase flow system is governed by the interface condition. In this study, the ratio between the dynamic head and the surface tension was considered to be an important parameter for the interface stability; the ratio is given as

$$K^2 = \frac{\rho V^2 \delta}{\sigma}$$

where ρV^2 is the dynamic head in contact with the other phase and δ is a characteristic dimension of the flow structure. For a low viscosity liquid dispersed in a gas stream, δ is approximately equal to $(\sigma/g(\rho_f-\rho_g))^{\frac{1}{2}}$. Substituting δ into the ratio K gives the Kutateladze number

$$K = V_g\left(\frac{\rho_g^2}{g\sigma(\rho_f-\rho_g)}\right)^{\frac{1}{4}} \qquad (11)$$

Some experimental data indicate that the critical K value is around 3.2 for flooding in an air-water system (10).

Imura et al. (15) applied the potential flow theory to the counter-current flow inside a tube as shown in Fig. 2b. The governing equations for both phases in the flow are the Laplace equation for velocity potential

$$\frac{\partial^2 \phi}{\partial x^2} + \frac{1}{r} \frac{\partial}{\partial r} \left(r \frac{\partial \phi}{\partial r} \right) = 0 \tag{12}$$

and Bernoulli's equation

$$\frac{P}{\rho} = \frac{\partial \phi}{\partial t} - \frac{1}{2} \left[\left(\frac{\partial \phi}{\partial x} \right)^2 + \left(\frac{\partial \phi}{\partial y} \right)^2 \right] - gx + \text{constant} \tag{13}$$

Boundary conditions are:

$$r = R \quad , \quad \frac{\partial \phi_f}{\partial r} = 0 \text{ (at the tube surface)}$$

$$r = o \quad , \quad \frac{\partial \phi_g}{\partial r} = 0$$

$$r = R - \delta \quad , \quad - \frac{\partial \phi_i}{\partial r} = \frac{\partial \eta}{\partial t} + V_i \frac{\partial \eta}{\partial x}$$

where i = g and f, and

$$P_f - P_g = \sigma \left[\frac{\partial^2 \eta}{\partial x^2} \Big/ \left(1 + \left(\frac{\partial \eta}{\partial x} \right)^2 \right)^{3/2} - \frac{1}{R - \delta + \eta} \right] \text{ (interfacial pressure)}$$

Here the surface disturbance is assumed to be $\eta = \eta_o(t)$ Sin $k(x - ct)$. Equation (12) was integrated for both the liquid and the gas phase with appropriate boundary conditions. The resulting ϕ_g and ϕ_f were substituted into equation (13),

with additional approximations, to obtain a stability equation based on the growth rate of $\eta(t)$:

$$\frac{d^2\eta_o}{dt^2} - \beta^2\eta_o = 0 \tag{14}$$

where β is a complicated expression of modified Bessel functions and fluid properties.

The stability criterion for Eq. (14) is $\beta^2 \leqslant 0$. With further manipulations, this led to the final result:

$$V_g + V_f = \sqrt{\frac{\sigma}{\rho_g}\left(k - \frac{1}{R - \delta}\right)} \tag{15}$$

Comparisons between experimental data and the flooding correlation derived from Eq. (15) showed good agreement except for a very high liquid flow rate. Further discussion of Eq. (15) is deferred to Section 3.

Chung (16) neglected the tube curvature effect and represented the flow as a two-dimensional plane flow shown in Fig. 2c. By applying the small perturbation method, the author reduced the Laplace equation for the velocity potential to:

$$\frac{\partial^2\phi'}{\partial x^2} + \frac{\partial^2\phi'}{\partial y^2} = 0 \tag{16}$$

and Bernoulli's equation to:

$$\frac{p'}{\rho} = -\frac{\partial\phi'}{\partial t} - \bar{V}\frac{\partial\phi'}{\partial y} - gy' \tag{17}$$

with boundary conditions

$$x = -h \quad , \quad \frac{\partial\phi'_f}{\partial x} = 0$$

$$x = H-h \quad , \quad \frac{\partial \phi'_g}{\partial x} = 0$$

$$x = \eta \quad , \quad \frac{\partial \eta}{\partial t} + \bar{V}_i \frac{\partial \eta}{\partial y} = \left.\frac{\partial \phi'_i}{\partial x}\right|_{x=\eta}$$

where i = f and g, and

$$p'_f - p'_g = \sigma \frac{\partial^2 \eta}{\partial x^2} \quad \text{(interfacial pressure)} \tag{18}$$

where (') and ($\bar{}$) denote the perturbation and time average component respectively, and $\eta = \eta_o \sin k(y - ct)$. Assuming the perturbation ϕ' can be expressed as $X(x) \cos k(y - ct)$ and substituting it into Eq. (16) with the appropriate boundary conditions, ϕ'_f and ϕ'_g were obtained. The small disturbance pressures p'_f and p'_g were then solved in terms of ϕ'_f and ϕ'_g. With additional manipulations, and an application of the kinematic wave theory, the interface pressure boundary condition, Eq. (18), was reduced to:

$$\frac{\rho V^2}{1-\alpha}\left(1 - \frac{2\delta^*}{1-\alpha}\right) + \frac{\rho V^2}{\alpha 3}\left(1 + \frac{2\delta^*}{\alpha}\right) = \frac{1}{c_1}\left(\frac{\lambda\rho}{2\pi} + \frac{2\pi\sigma}{\lambda}\right) \tag{19}$$

where $\alpha = \frac{H-h-\eta}{H}$ (void function) and $\delta^* = \eta/H$. With successive maximizations and an application of the Taylor instability critical wavelength (28), $\lambda_{cr} = C_2[\sigma/g(\rho_f - \rho_g)]^{\frac{1}{2}}$, where $C_2 \geq 2\pi$, Eq. (19) can be expressed as

$$K_g^{\frac{1}{2}} + K_f^{\frac{1}{2}} = C_K \tag{20}$$

where the Kutateladze number, $K_i = V_i[\rho^2_i/\sigma g(\rho_f - \rho_g)]^{\frac{1}{4}}$, i = f and g, and $C_K \geq \pi^{\frac{1}{4}}$. By semi-empirically choosing C_K to be $C_{11} \tanh [C_{12}(D^*)^{\frac{1}{4}}]$, Eq. (20) can be modified into:

$$K_g^{\frac{1}{2}} + m\, K_f^{\frac{1}{2}} = C_{11} \tanh[C_{12}(D^*)^{\frac{1}{4}}] \tag{21}$$

where m, C_{11} and C_{12} are empirical constants and D* ($=D[g(\rho_\ell - \rho_g)/\sigma]^{\frac{1}{2}}$) is the Bond number. Experimental data were correlated successfully by Eq. (21) with properly chosen empirical constants.

3.0 EXPERIMENTAL INVESTIGATIONS

As in many other fields of research, experimental works are the most important source of information in the investigation of the flooding phenomenon. In the late 1930's, to improve the design of chemical plants, experiments were performed to investigate flooding in packed towers or columns (1,2). Flooding experiments in single channels were later employed for studying the more fundamental aspects of this phenomenon. Extensive tests have been performed in this geometry and they have generated many interesting results. An obvious drawback of the single-channel geometry is that it oversimplifies the actual geometry involved. Studies of flooding in simulated PWR and BWR geometries were also performed (5,6); a discussion of these studies is presented in Section 4.

Because of the complex nature of the problem, studies up to date have not produced a clear picture of the flooding phenomenon. A general systematic experimental procedure also seems to be lacking in the flooding investigation. This inconsistency has resulted in conflicting reports which exist throughout the literature. The majority of the disagreements center on the dependence of the flooding velocities on test channel geometries and on physical properties of the fluids. These discrepancies may be partly caused by the difficulty in isolating a particular parameter without affecting others; this is especially true for liquid physical properties. Moreover, flooding involves highly unsteady flow behaviors; it is difficult to determine precisely the onset of flooding. Many investigators have established different criteria for the inception of flooding, another factor contributing to some of the disagreements in the existing data. A review of the experimental methods, existing results and flooding correlations are given. A discussion of the parametric dependence of these correlations follows.

3.1 Experimental Methods

The basic arrangement for the single-tube experiment is shown in Fig. 3. The liquid was introduced into the tube either through porous injection or top flood entry (see Fig. 3a,b). The porous injector is generally considered to be the

smoothest entry since it generates the least disturbance in the liquid flow (24). Top flood entry, on the other hand, has various degrees of entry effect, depending on the actual geometry (8,16). There were also two modes of feeding the gas into the test channel: either by issuing gas into the lower plenum or through a nozzle which is alined with the text channel axis (see Fig. 3d).

Flooding in the test channel was reached either by gradually increasing the gas velocity for a fixed liquid flow rate (Mode 1) or by increasing the liquid flow rate for a fixed gas velocity (Mode 2), as described in Section 1.1. The onset of flooding was determined mainly by visual observations, but a few investigators also used the gas pressure drop as a second criterion.

3.2 Flooding Correlations

Earlier works on flooding in packed towers were done by Lobo et al. (2) and Sherwood et al. (1). These authors did not correlate their results into a parametric equation but only presented them as a graph of

$$\frac{j_g}{g}\frac{a}{F^3}\frac{\rho_g}{\rho_f}\mu^{0.2} \quad \text{vs.} \quad \frac{\rho_f j_f}{\rho_g j_g}\left(\frac{\rho_g}{\rho_f}\right)^{1/2} ,$$

where a/F^3 is a characteristic inverse length (area/void volume).

Flooding tests were done by Kami et al. (29) for water, a Millet jelly solution and a soap solution flowing against air in tubes with a diameter of 1.89, 3.16, 4.18 and 4.9 cm (0.75, 1.25, 1.65 and 1.93 in., respectively), and a length of 2.5 m (8.2 ft.) with a sharp entry. The range of Re_f ($\equiv \rho_f V_f \delta/\mu_f$) tested was between 50 and 700. The following empirical equation was obtained:

$$\frac{\rho_g j_g}{\rho_f j_f} = 198\left(\frac{4\rho_f j_f}{\pi D \mu_f}\right)^{-1.225}\left(\frac{\delta}{D^2\rho_f g}\right)^{-0.23}\left(\frac{\mu_g}{\mu_f}\right)^{0.71}\left(\frac{\rho_g}{\rho_f}\right)^{0.13}\left(\frac{D^3\rho_f{}^2 g}{\mu_f}\right)^{0.231} \qquad (22)$$

where δ is the Nusselt film thickness, $\left(\frac{3\mu_f j_f D}{g\rho_f}\right)^{1/3}$.

Feind (30) tested flow combinations of air-water and air-diethylene glycol solution over a liquid Reynolds number range of 0.15 to 3000. Three tube sizes were

used, 2.0 cm (0.79 in.) in diameter, 2.5 m (8.2 ft.) in length; 5.0 cm (1.97 in.) in diameter, 0.96 m (3.15 ft.) in length; and 5.0 cm in diameter, 2.5 m in length, all with a conic nozzle entry. The following correlation was given:

$$M \left(\frac{Re_g}{Re_f{}^n}\right) \left(\frac{\rho_g}{\rho_f}\right)^{2/5} \left(\frac{\mu_g}{\mu_f}\right)^{3/4} + 1.4 \times 10^4 = 1300 \left(\frac{R}{\delta}\right)^{5/4} \qquad (23)$$

where R is the tube radius and $Re_g = \frac{\rho_g V_g (D-\delta)}{\mu_g}$. For $Re_f < 400$, M = 58.2, n = 1/3; for $Re_f > 400$, M = 157.7, n = 1/2.

Wallis (8) considered a balance of inertial and hydrostatic forces and defined dimensionless velocities for the two-phase flow components as:

$$j_f^* = j_f \rho_f^{\frac{1}{2}} [Dg(\rho_f - \rho_g)]^{-\frac{1}{2}}$$

and

$$j_g^* = j_g \rho_g^{\frac{1}{2}} [Dg(\rho_f - \rho_g)]^{-\frac{1}{2}} \quad .$$

He then correlated the experimental data into an empirical equation as:

$$j_g^{*\frac{1}{2}} + j_f^{*\frac{1}{2}} = c \qquad (24)$$

where c is an experimental constant. Equation (24) was later modified into:

$$j_g^{*\frac{1}{2}} + m j_f^{*\frac{1}{2}} = c \qquad (25)$$

where m is a second experimental constant. For most cases, m has a value of 0.8 to 1.0 and c ranges from 0.7 to 1.0. Equation (25) is one of the more frequently used correlations. Many experiments have been performed to test its validity under various conditions. Wallis (8) first performed his experiment with Perspex tubes of nominal diameters of 1.27, 1.91, 2.54 and 5.1 cm (1/2, 3/4,

1 and 2 in.). All tubes were 1.22 m (4 ft.) long. Three types of flanges, sharp edge, step and nozzle, were used to secure the tube between the top and lower plenum. Air and water were used as test fluids. The onset of flooding (Mode 2) was determined visually, taken at the instance when the liquid flow became chaotic with a large interfacial wave formation. The author concluded that the tube diameter and entrance condition, reflected in the constant c, are important parameters in flooding. The constant c takes a larger value for smoother entry. If flooding is a result of hydrodynamic instability, as suggested by many authors (13-16,24,27), it is intuitive to expect the influence of the liquid entry on the flooding point. Chung (16) also observed marked differences in flooding velocities for the same size tubes but having different tube end finishes. Flooding velocities were found to be higher for a tapered tube end than that for a straight flushed end.

The tube hydraulic diameter dependence in Eq. (25) has drawn some criticism regarding its validity (9,10,16,18). Wallis suggested recently that in some instances, D should be replaced by an appropriate length such as the flow circumference, the film thickness or a characteristic wavelength involving surface tension.

Wallis (32) did a subsequent investigation of the viscosity effect on flooding with the air-water, air-ethylene glycol and air-glycerol combinations in a 1.91 cm (3/4 in.) ID tube. The viscosity was found to reduce the liquid flooding velocities.

Hewitt and Wallis (24) employed porous injection and extraction to completely eliminate the liquid entry effect. Data were collected for air-water flow in a 3.18 cm ID (1-1/4 in.) bore acrylic resin pipe. The inception of flooding (Mode 2) was taken at the instance when the liquid was carried up beyond the injector. These authors showed that without entry effect and little disturbance in the flow, the value of c is near unity.

English et al. (33) performed steam-water flooding tests in a single tube updraft partial condenser made of jacket 1.83 m (6 ft.) in length, 1.91 cm (3/4 in.) in diameter stainless steel tubes with four different diagonal tube end cutting (0°, 30°, 60° and 75°). The criterion for the onset of flooding (Mode 1) was the large gas pressure drop across the tube. These authors correlated their results by

$$\rho_g j_g = \frac{1550 D^{0.3} \rho_f^{0.46} \rho_g^{0.5} \delta^{0.9}}{\mu_f^{0.14} (\cos\Theta)^{0.32} \left(\frac{\rho_f j_f}{\rho_g j_g}\right)^{0.07}} \qquad (26)$$

where Θ is the angle of diagonal cutting, which was found to have a stabilizing effect on the flooding velocities. It was thought that the diagonal cutting of the tube end had probably minimized the liquid accumulation around the exit edge, hence, allowed a larger liquid flow rate.

Clift et al. (25) tested air-water and air-glycerol flows in Perspex tubing with a nominal ID of 3.18 cm (1-1/4 in.) and a length of 3.66 m (12 ft.) and with a porous injector. The flooding point (Mode 1) was determined both visually and by direct measurement of the gas pressure drop. The Wallis correlation with $c = 0.79$ and $m = 0.34$ or $(j_g^*)^{\frac{1}{2}} + 0.34(j_f^*)^{\frac{1}{2}} = 0.79$ was found to give good agreement with the air-water data obtained. The liquid flooding velocities were shown to decrease at higher viscosities.

Air-water, steam-water and air-sugar solution flows were tested by Tobilevich et al. (18) in an evaporator with two tubes, 3.27 cm (1.29 in.) and 5.25 cm (2.07 in.) in diameter and 3 m (9.84 ft.) in length, and in a 24 tube evaporator, 3.0 cm (1.18 in.) in diameter and 2.5 m (8.2 ft.) in length. The onset of flooding was taken at the point of flow reversal. These authors correlated their results by:

$$Fr = a \exp\left\{bK_g \left(\frac{\rho_g}{\rho_f}\right)^{0.2}\right\} \qquad (27)$$

where Fr is the Froude number, defined as

$$Fr = \frac{\Gamma_v}{(gD^3)^{\frac{1}{2}}}$$

and

$$\Gamma_v = \rho_f \frac{g - \frac{4\Delta P_c}{L}}{3\mu_f} - \frac{\tau_i}{2\mu_f} \delta^2$$

ΔP_c is the pressure drop at the onset of flooding, τ_i is shear stress at the interface, L is the tube length, and K_g is the Kutateladze number. For $Fr > 0.012$, $a = 0.129$, $b = -14.14$; and for $Fr < 0.012$, $a = 0.0653$, $b = -10.12$. These authors attempted to investigate the effects of viscosity by using a sugar solution; the results were inconclusive since the difference between the density of a sugar solution and that of water is also appreciable.

The Kutateladze number K was also used by Pushkina and Sorokin (10) to correlate their results. These authors designed two separate test stands: one had a glass tube of 30.9 cm (12.17 in.) ID with a porous injector, and the other had glass tubes of different diameters (6.2, 8.8, 9 and 12.2 mm, or 0.24, 0.35 and 0.48 in., respectively) with a nozzle entry. Air and water were used as test fluids. The onset of flooding (Mode 1) was visually determined to be at the instance when a significant flow reversal occurred. Only the air velocity was measured; the critical air velocity was found to correspond to $K \approx 3.2$, independent of the hydraulic diameter D. This independence on D is contrary to Wallis' results (8). However, their data for the tubes with a diameter of less than 9 mm gave k values lower than 3.2. These authors attributed the difference to experimental errors. These authors also reported that the flooding velocities are nearly the same as the deflooding velocities which is not in agreement with other investigators' findings (7,13,25). Deflooding is used to describe the recovery of a counter-current flow from a co-current flow after the onset of flooding.

It was reported (12) that Makkencherry did a series of studies on flooding with air-water flow in a tube size range of 1.91 cm to 13.97 cm (0.75 in. to 5.5 in.). The results showed that the flooding velocities are independent of tube diameters greater than 5.08 cm (2 in.). Wallis and Makkencherry (34) did hanging film experiments with air and water in Plexiglas tubes with diameters between 6.4 mm (0.25 in.) and 14 mm (5.5 in.) with nozzle entry. Based on their data, these authors speculated that Pushkina and Sorokin's results may be the limit for which the contact angle is very small (45° for glass, 60° for Plexiglas) and that suitable experiments could establish a family of curves each characterized by a different value of contact angle. Lovell (9) showed that in a large size Plexiglas tube (6 inches and above) the critical Kutateladze number for zero penetration depth was between 3.13 and 3.28. It seems that for a small tube size, the liquid contact angle may be an important factor in flooding.

Another flooding correlation was proposed by Diehl and Koppany (35):

$$j_g = a\{f_1 f_2 \ (\sigma/\rho_g)^{1/2}\}\ b \tag{28}$$

where f_1 depends on the ratio of tube diameter to surface tension and f_2 depends on the ratio of liquid mass flux to gas mass flux. Hewitt (36) showed that Eq. (28) did not agree well with his results.

Flooding rates in regular packings were determined by Alekseev et al. (37). By correlating their data with results of other investigators, these authors showed that the critical gas velocity is given by:

$$K_g = 0.32\ Fr^{-0.22}\ We^{-0.26} \tag{29}$$

where the Froude number Fr is defined as $\dfrac{Q_f(\rho_f-\rho_g)^{3/4}}{g^{1/2}\ \sigma^{3/4}}$, Q_f is the liquid flow rate, and the Weber number We is $\dfrac{\sigma}{(\rho_f-\rho_g)D_{eq}^3}$.

Flooding data were collected for a glass tube with a conic nozzle entry and nitrogen-water flow by Gromles et al. (17). Large L/D combinations were used: for 4 mm (0.16 in.) and 6 mm (0.24 in.) diameter tubes, L/D were 10, 25, 50 and 100; for 13 mm (0.51 in.) diameter tube, L/D were 50 and 100; for 25 mm (0.99 in.) diameter tube, L/D was 50. The onset of flooding (Mode 1) was determined both visually and by direct measurement of the gas pressure drop in the test section. These authors correlated their results based on their analytical result, Eq. (2), discussed in Section 2:

$$j_g = 1.15 \left[\frac{\rho_f}{\rho_g} \frac{g\delta}{0.006 + \dfrac{200\ \delta^2}{(\mu/\mu_R)^{0.44}}}\right]^{1/2} \tag{30}$$

where μ_R is a reference viscosity. These authors concluded that the effect of the tube diameter and L/D ratio on the critical gas velocity is small.

Sakhuja (38) measured the flooding limit in wickless heat pipes and found that the Wallis correlation gave good agreement with his experimental data. Hagi (39) and Lovell (9) performed flooding tests in Plexiglas tubes to recheck the Wallis correlation; Lovell showed that for a tube size larger than 15.24 cm (6 in.), the Wallis correlation failed to hold. Dukler and Smith (11) used air-water flow in a 5.1 cm (2 in.) ID Plexiglas tube (1.6 m. or 5-1/4 ft. long) with a smooth nozzle entry on both the top and bottom end. These authors reported good agreement between their results and the Wallis correlation with c = 0.88.

Hewitt (36) did another series of experiments with porous injection. Two tube lengths (1.22 and 2.44 m or 4 and 8 ft.) and two tube diameters (1.27 and 3.18 cm or 1/2 and 1-1/4 in.) were used. The lower end of the tubes were cut either straight or at a 30° angle. Water, glycerol (38% and 67%) and silicon fluid were used with air. The flooding point (Mode 2) was determined visually to correspond with the formation of a highly disturbed and "jiggling" liquid film in which waves travelled upwards. Contrary to his earlier findings (40), the author showed that there was a small length effect, which agreed with the findings by Shires and Pickering (41) and Grolmes et al. (17). Tube diameter effect was also found to exist. The diagonal cutting of the tube end was observed to increase the flooding velocities, as observed by English et al. (33). Hewitt also showed that viscosity has a destabilizing effect and that surface tension has a stabilizing effect.

Imura et al. (15) used acrylic resin tubes with a nozzle entry of 1m (3.28 ft.) long and inside diameters of 1.12, 1.60, 2.10 and 2.42 cm (0.44, 0.63, 0.83, and 0.95 in., respectively). Water, ethyl-alcohol, ethylene-glycol and n-neptane were used as flowing liquids against air over a liquid Reynolds number range of 2.7 to 4230. The onset of flooding (Mode 1) was determined both visually (a change in the flow pattern) and by measuring the gas pressure drop. Equation (15), derived analytically by these authors, was modified to fit their experimental data:

$$\frac{G}{L}\left(1+\frac{L}{G}\frac{\rho_g}{\rho_f}\frac{S_g}{S_f}\right)=\frac{S_g}{S}\frac{1}{L}\left(\frac{\rho_g\sigma}{S}\right)\left[\zeta-\left(\frac{1}{R/\delta-1}\right)^{1/2}\right]^{1/2} \qquad (31)$$

where $LS=\rho_f j_f S_f$, $GS=\rho_g j_g S_g$, $S=\pi D^2/4$, $S_f=\pi D\delta(1-\delta/D)$, $S_g=(\pi D^2/4)(1-2\delta/D)^2$, $\zeta=0.046\,(D^2\rho_f g/\delta)^{1/2}\,(\mu_f/\mu_g)^{0.12}$. For $Re_f \leq 400$, $\delta=(3\mu_f^2/\rho_f^2 g)^{1/3}Re_f^{1/3}$;

$Re_f > 400$, $\delta = 0.369\ (3\mu_f^2/\rho_f^2 g)^{1/3} Re_f^{1/3}$, where $Re_f = LD/4\mu_f(1-\delta/D)$.

Suzuki and Ueda (7) did extensive testing for air flow against water, glycerol and sec -octynol covering a wide range of viscosities, from 9.0×10^{-4} to 2.4×10^{-2} N sec/m^2, surface tension, from 0.037 to 0.068 N/m, tube diameters, from 1.0 cm (0.39 in.) to 2.88 cm (1.13 in.) and lengths, from 0.5 m (1.64 ft.) to 2 m (6.56 ft.). Acrylic resin tubing with porous liquid injection was used. The onset of flooding (Mode 1) was determined visually. A correlation based on the Froude number was obtained:

$$Fr = A\log_{10} X + B \tag{32}$$

where $Fr = [\rho g(V_g + V_f)^2/\rho_f\ g\ \delta]$; V_g and V_f are the actual velocities, and δ is the mean film thickness.

For tube length L_d = 0.5 m, A = 0.766, B = 18.37; L_d = 1.0 m, A = 8.29, B = 19.18; L_d = 1.5 m, $Re_f \leq 350$ or $\mu_f \geq 3 \times 10^{-3}$ N sec/m^2, A = 8.29, B = 19.18, and $Re_f > 350$ or $\mu_f < 1 \times 10^{-3}$ N sec/m^2, A = 11.94, B = 25.0; L_d = 2.0 m, $Re_f \leq 350$ or $\mu_f > 3 \times 10^{-3}$ N sec/m^2, A = 8.29, B = 19.18, and $Re_f > 350$ or $\mu < 1 \times 10^{-3}$ N sec/m^2, A = 14.86, B = 29.7. Also, $X = Re_f^{-1/3}(\rho_f g D^2/\sigma')^{1/4}(\mu_g/\mu_f)^{2/3}$ and $\sigma' = \sigma + 15\ |\sigma - 0.05|$ N/m; where $Re_f = \dfrac{\rho_f j_f D}{\mu_f}$. These authors reported that tube diameter D and length L affect the flooding velocities as observed by Wallis (8) and Hewitt et al. (40), respectively. However, viscosity was found to have a stabilizing effect, contrary to the findings of Wallis (32), Clift et al. (25) and Hewitt (36). Surface tension was found to have a complicated effect; both the largest and the smallest surface tension value gave lower flooding velocities than those of intermediate values.

Chung (16) conducted air-water tests for four different tube ID: 1.59, 3.18, 4.60 and 6.99 cm (5/8, 1-1/4, 1-10/13, and 2-3/4 in.). The onset of flooding (Mode 1) was determined both visually (chaotic flow pattern) and by measuring the gas pressure drop. The author showed that for a 45° tapered tube end and nozzle air inlet, the data can be correlated by Eq. (21)

$$K_g^{1/2} + mK_f^{1/2} = (11 \tanh [C_{12}\ (D^*)^{1/4}]$$

with m = .8, C_{11} = 2.11 and C_{12} = 0.9, or:

$$K_g^{1/2} + 0.8K_f^{1/2} = 2.1 \tanh [0.9 (D^*)^{1/4}] \quad . \tag{33}$$

For a straight flushed tube end, the constant C_{12} was found to be 0.8. When the air was introduced through the lower plenum, the data for a tapered tube end were correlated by:

$$K_g^{1/2} + 0.65K_f^{1/2} = 1.79 \tanh [0.9 (D^*)^{1/4}] \quad , \tag{34}$$

and for a straight flushed tube end, C_{12} = 0.8. The author reported that the gas entry effect dominated over that of the liquid at small liquid flow rates and vice versa. The tube diameter effect was found to be insignificant when the entry was smooth. Surface tension was found to have a stabilizing effect.

3.3 Parametric Dependence

Table 1 summarizes the various flooding studies discussed in Section 3.2. The parametric dependence of the flooding correlations is not well established. Investigators have reported conflicting findings regarding the geometric and fluid property effects on the flooding characteristics.

The tube entry geometry seems to have a definite effect on flooding: flooding velocities decrease with a less smooth entry geometry. Chung (16) noted that when a gas was introduced into the tube through a nozzle (see Fig. 3d), the flooding velocities increased. This indicates that the gas entry condition also affects the flooding characteristics.

Tube diameter and tube length effects are not clear; the number of literature citations reporting definite effects roughly equal those reporting little or no effect. Analyses by Grolmes et al. (17), Shearer and Davidson (13), Cetinbudaklar and Jameson (14), Kutateladze (27) and Chung (16) showed no explicit diameter dependence for the flooding velocity; however, analyses by Imura et al. (15) and Wallis and Kuo (19) indicated the opposite.

Although a number of correlations contain the viscosity term, most of these correlations have little direct experimental support. Experimental evidence

given by Wallis (32), Clift et al. (25) and Hewitt (36) showed that viscosity has generally a destabilizing effect, but that given by Suzuki and Ueda (7) presented the opposite evidence. Cetinbudaklar and Jameson's analysis (14) indicated that viscosity is stabilizing, while Chung (16) did a qualitative analysis showing a destabilizing effect of viscosity.

Surface tension, which is not included in the Wallis correlation, may also be important to the flooding characterization. Hewitt (36) and Chung (16) showed that surface tension has a stabilizing effect which agrees with Cetinbudaklar and Jameson's (14) and Chung's (16) analyses. Suzuki and Ueda (7) reported no general trend for the surface tension effect.

Film thickness appeared in Grolmes et al's. (17), Feind's (30) and Imura et al's. (7) correlation. The role of film thickness in the flooding phenomenon is still not clear. Cetinbudaklar and Jameson (14) gave a qualitative discussion on the film thickness arguing that film thickness influences the viscous damping of interface disturbance: the thinner the film, the more effective the damping; hence, the liquid flow can sustain a higher gas velocity. But, for a given size of pipe, a thinner film means a lower liquid flow rate. Existing experimental data show that the critical gas velocity is higher for a lower liquid flow rate. The interrelationship between the hydraulic diameter and the film thickness makes it very difficult to isolate the effect of the latter.

4.0 EXTENDED PROBLEMS IN FLOODING

Apart from the hydrodynamics in single channel flooding, there exists a wide spectrum of problems associated with the flooding phenomenon. In LOCA application, of immediate concern is the vapor condensation effect in a flooding situation. Flooding in simulated PWR downcomer and BWR geometries (multichannel) is another topic of interest for attaining a more realistic assessment of the reactor safety analysis. Liquid entrainment effects and flooding in inclined channels are also of practical significance.

4.1 Vapor Condensation

Vapor condensation occurs during a LOCA when subcooled ECCS water flows downward against the updrafting steam. Such condensation can alter considerably the characteristics of flooding. Hence, in order to predict the flooding velocities to some degree of accuracy in a real situation, the existing studies on flooding based on hydrodynamic consideration must be modified to incorporate this effect.

Tien (42) examined the effect of vapor condensation on flooding characteristics. In his subcooled flooding model, the author incorporated this effect on liquid film surfaces by calculating the steam flow reduction, assuming that the condensation latent heat is balanced by the sensible heat needed to raise the temperature of the subcooled water to the saturation temperature. Then, the effective steam flow based on the Kutateladze number is:

$$K_{ge} = K_g - fK_f \left(\frac{c_p \Delta T_{subcooled}}{h_{fg}}\right)\left(\frac{\rho_f}{\rho_g}\right)^{\frac{1}{2}} \tag{35}$$

where f is the fraction condensed, determined empirically.

By substituting K_{ge} into the flooding correlation $K_g^{\frac{1}{2}} + K_f^{\frac{1}{2}} = 1.79$, based on the critical value of K_g as 3.2, a subcooled flooding correlation was obtained:

$$(K_g - Bf\Delta T_{sub}K_f)^{\frac{1}{2}} + K_f^{\frac{1}{2}} = 1.79 \qquad (36)$$

where $B = (\frac{c_p}{h_{fg}})(\frac{\rho_f}{\rho_g})^{\frac{1}{2}}$. The author concluded that liquid subcooling or vapor condensation has a stabilizing effect on flooding characteristics. Subcooling also introduces in the flooding curve a minimum point and positive-slope region which is unstable. This results in a hystersis effect.

Block and Crowley (43) investigated the subcooling effect on flooding in simulated PWR downcomer geometries. The effect of liquid subcooling was found to increase the liquid flooding velocities. These authors proposed a flooding correlation which takes into the account of the subcooling effect:

$$j_g^{*\frac{1}{2}} + mj_f^{*\frac{1}{2}} = c \qquad (37)$$

where $j_f^* = \rho_f j_f^{\frac{1}{2}}[(\rho_f - \rho_g)gW]^{-\frac{1}{2}}$, W = average annalus circumference and

$$j_g^* = j_{gc}^* + j_{gw}^* - j_{gcond}^* \qquad (38)$$

and

$$j_{gcond}^* = f(T_{sat} - T_f)\frac{c_p}{h_{fg}}[\frac{\rho_f}{\rho_g}]^{\frac{1}{2}} j_{f,in}^* \qquad (39)$$

where f is the fractional condensation efficiency,

$$f = [\frac{P}{P_a}]^{\frac{1}{4}}[\frac{1}{1 + bj_{f,in}^*}] \quad . \qquad (40)$$

The factor b in Eq. (40) has a value of 30 for cylindrical vessel, and P_a is the atmospheric pressure. In Eq. (38), j_{gc}^* is the steam flux generated from the core and j_{gw}^* is generated from the downcomer wall, and $j_{f,in}^*$ is the rate of liquid injection into the vessel. In Eq. (37) the coefficient c is set as 0.32, and m can be either empirically determined or given by $\exp[-5.6\, j_{f,in}^{*\,0.6}]$.

Jones (44) studied the subcooled counter-current flooding characteristics of the upper region of a simulated BWR fuel bundle. The onset of flooding in the upper region of a BWR fuel bundle with subcooled liquid injection is determined by

$$\dot{M}_{in_c} = \frac{\dot{M}_f c_p \Delta T_{sub}}{h_{fg}} \tag{41}$$

where $\dot{M}_{in_c}$ is the steam flow rate, $\dot{M}_f$ is liquid injection rate and ΔT_{sub} is the degree of subcooling. Assuming a single condensation front for the inlet steam flow, then as steam flow rate increases, the front will propagate up along the bundle. When the condensation front is at the upper tie plate, the corresponding steam flow rate is given by Eq. (41). The author concluded that the subcooled flooding model proposed by Tien (Eq. (35)) is adequate, for increasing steam flow, if the condensation efficiency is set to unity for $\dot{M}_{in} < \dot{M}_{in_c}$ and to zero for $\dot{M}_{in} > \dot{M}_{in_c}$.

4.2 Liquid Entrainment

The liquid entrainment phenomenon, especially the criteria for the inception of entrainment and the liquid droplet distribution, has been investigated by many researchers. Some have dealt with the effects of liquid entrainment on other physical phenomena in which entrainment invariably arises, primarily in LOCA reflooding. Again these studies concerned themselves with the inception criteria, droplet size distribution and carry over fraction correlation (45). But, no work exists studying the entrainment effect on counter-current flooding.

Dukler and Smith (11) performed flooding experiments in single tube. From their observations, these authors suggested that the onset of liquid entrainment is associated with the onset of flooding: the initiation of entrainment causes flow reversal as a result of liquid droplets being carried upward in the gas stream. Two types of entrainment were observed: (1) falling film entrainment in which the entrainment takes place well below liquid entry, and (2) liquid entry region entrainment in which entrainment takes place at the entry location. The former occurs at low liquid flow rate and the latter occurs at high liquid flow rate.

Chung (16) made an extension in his flooding modeling (see Section 2.2.3) to include entrained droplets in the gas flow. The result of the analysis qualita-

tively showed that liquid entrainment reduces the flooding velocities in the low liquid flow regime. Experimental result obtained by the author also showed this qualitative trend. A possible explanation to this trend is that the additional momentum flux from the entrained droplets in the gas stream caused the observed shift. At high liquid flow rates, the effect of this additional momentum flux diminishes. A comprehensive study is needed to fully understand this effect.

4.3 Flow Inclination

Hewitt (36) performed experiments in inclined tubes and showed that the effect of tube inclination is complicated. In general, the liquid flooding velocity increased and then decreased as the inclination angle went from 90° (vertical) to 10°. The author cited this as a direct evidence of the film thickness effect. A qualitative argument was given: with a slight inclination, a considerable mal-distribution of the film flow can take place, which causes local thickening of the liquid film around the lower portion of the tube circumference. For a given liquid flow rate, this would mean that the average film thickness would decrease considerably since film thickness rises at a fractional power of the local flow rate. Thus, if flooding is associated with thickening of the liquid film, inclining the tube slightly will increase the liquid flooding velocities. But further inclination reduces the gravitational force on the film, which causes the liquid film to become thicker, hence, lower flooding velocities. However, it should be noted that annular film flows will degenerate into stratified flow as the inclination angle decreases to a smaller value.

Boyadjiev et al. (46) solved a laminar boundary layer problem at the interface of a counter-current stratified flow by a perturbation method. The velocity profiles generated in this solution agreed well with the experimentally measured profiles.

4.4 Flooding in PWR Downcomer Geometries

Both air-water and steam-water tests have been performed in simulated PWR geometries (12). The two basic geometries employed in these tests were:

A) An annular geometry, composed of two concentric cylinders with various "hot" and "cold" leg attachments, scaled roughly linearly to a PWR geometry.

B) An "unwrapped annulus" geometry, composed of two flat plates with various leg attachments. This arrangement was justified by the premise

of the small ratio of the annulus gap to the vessel diameter.

4.4.1 Air-water Flooding

Naff and Whitebeck (47) employed the annulus geometry with a radial gap of 0.9, 1.2 and 1.7 cm (0.37, 0.49 and 0.68 in.) and downcomer annulus length of 15.2, 63.5, 86.4 and 172.7 cm and (6, 25, 34 and 68 in.). These authors showed that their results can be correlated by $j_g^{*\frac{1}{2}} + 0.8 j_f^{*\frac{1}{2}} = 0.9$. Length effect was not observed except for the L/D ratio of unity. Additional tests were performed by Hanson et al. (48) with radial gaps ranging from 0.9 to 3.87 cm (0.35 to 1.58 in.) and various L/D ratios. These authors observed that for $L/D \approx 1$ with high liquid flow rates, the limiting value of j_f^* is dependent on the rate at which the liquid was injected into the vessel. No significant effects were observed for geometrical changes, such as changing L/D ratio or removing the hot leg simulator.

Crowley et al. (49) performed flooding tests in the "unwrapped annulus" geometry with a 0.95 cm (0.375 in.) gap (1/30 scale to a PWR). The flooding data was correlated by $j_g^{*\frac{1}{2}} + j_f^{*\frac{1}{2}} = 0.94$, independent of the liquid injection rate. These authors noted that the insertion of "hot" legs into the annulus section influenced the flooding in the annulus.

Cudnik and Wooton (50) used 1/15 scale model of a PWR with a 1.51 cm (0.594 in.) gap and "hot" leg attachments. These authors correlated their results by $j_g^{*\frac{1}{2}} + 0.77 j_f^{*\frac{1}{2}} = 0.8$. Air-water data for 1/30 scale model PWR downcomer were also taken (49). These data were correlated by $j_g^{*\frac{1}{2}} + j_f^{*\frac{1}{2}} = 0.94$, same as the correlation obtained for the unwrapped annulus geometry (49).

4.4.2 Steam-Water Tests

Experiments with steam-water in simulated PWR downcomer have been performed with 1/30 scale at Dartmouth College, 1/15 scale at Battelle Columbus, 1/30 scale and 1/15 scale by Creare, Semiscale by INEL, and 1/5 scale by Combustion Engineering. Compiling the test results showed that j^* (a dimensionless mass flux with average annulus circumference as the characteristic length) or K are the proper dimensionless variables to correlate the test results. The annulus width does not seem to be a characteristic dimension in these situations. Block and Schrock (5) and Wallis (12) both gave a comprehensive review on steam-water and air-water testings in model PWR downcomer.

4.5 Multichannel Flooding

Flooding tests in parallel channels were performed by Hagi (39). The results showed that the Wallis correlation as given in Eq. (25) did not give good agreement. The author suggested that an equal pressure drop in both channels may be a good constraint on the flooding limit. Speyer and Kmetyk (51) did a four-channel flooding test and also concluded that the Wallis correlation became inadequate after the first channel had been flooded. It appears that all single-channel correlations must be modified to incorporate the multichannel effect.

A computation scheme was proposed by Speyer and Kmetyk (51) to obtain flooding points in a four-channel situation: the first flooding point is obtained by applying the Wallis correlation and successive flooding points are obtained by assuming the liquid flows to be distributed evenly in the penetrated channels, this giving j_f in the remaining channels. In the penetrated channels j_g is calculated from the Wallis correlation. Requiring that the pressure drop in the flooded channels be the same as that in the penetrated ones, the gas flow rate in the flooded channel can be solved. The last channel flooding is solved by directly applying the Wallis correlation.

These authors conceded that there are many limitations in such a computation scheme. A major flaw arises from the assumption that the flow is equally distributed in penetrated channels. It has been observed experimentally by both Hagi (39) and Speyer and Kmetyk (61) that hystersis takes place between flooded and penetrated channels. But the results from the computation did agree fairly well with Speyer and Kmetyk's experimental results within the scope of their experiment.

Ueda and Suzuki (21) performed air-water flooding experiments in annular and rod bundle geometries. For annular geometry, these authors tested three different annulus width and found that the flooding velocity decreases with decreasing annulus width. For rod bundle geometry, both the rod-shroud and rod-rod clearance were varied. By introducing an equivalent diameter

$$Deq = \frac{4A_s}{\pi(D_i + \pi d)}$$

where A_s is the total flow cross sectional area, D_i the inside diameter of shroud, d the rod diameter, and n the number of rods.

Flooding results from annulus and rod bundle were correlated by Eq. (32) with A = 8.29 and B = 19.18.

4.6 Flooding in BWR and PWR Upper Core Structure

Tobin (52) performed experiments with steam and water in a simulated BWR fuel bundle to obtain information on flooding in the upper tie plate open area. The fuel bundle size was 7 x 7. Sun and Fernandez (53) correlated Tobin's data with

$$K_g^{1/2} + K_f^{1/2} = (3.2)^{1/2} \quad . \tag{42}$$

Jones (44) performed another series of tests with steam-water in simulated 8 x 8 BWR fuel bundle to study the flooding characteristics in the upper region of a BWR fuel bundle. Test results showed that the method of liquid injection moderately influences the flooding results. However, the steam inlet geometry was found to strongly affect the flooding data. Measurements showed that the tie plate pool temperature distribution is also affected by the method of liquid injection.

Mohr and Jacoby (54) investigated the flooding phenomena through the end box and upper core support plate of KKU (German PWR of Kraftwerk Union Design) design. There appeared to be little effect on the flow from the support column. Test results showed that the critical Kutatuladze value, Kg, to achieve zero liquid penetration has values between 4 and 4.5, which is greater than the 3.2 limit determined in previous investigations (9,10). Mohr and Lopez (55) performed additional three series of tests in the KKU support column test apparatus to investigate (1) the effect of air injection method, (2) the behavior of the water injector below the simulated core, and (3) the effect of the upper plenum froth density and core liquid entrainment on the flooding behavior.

The flooding results obtained in the first test series with nonsymmetric air injection differed very little from those obtained with symmetric air injection. The second test series did not yield useful results. The third test series displayed little dependence on the density of the upper plenum froth. Core liquid

entrainment appeared to have significant effect on flooding behavior. Overall data correlation was improved when the amount of core liquid entrainment was included as an independent variable in the correlation equation:

$$K_f^{\frac{1}{2}} = -0.061\ K_g^{\frac{1}{2}}(QW1) - 0.924\ K_g^{\frac{1}{2}} + 0.111\ (QW1) + 2.089 \qquad (43)$$

where QW1 is the core liquid entrainment rate. The authors conceded that the application of Eq. (43) needs to be further investigated.

4.7 Counter-Current Annular Flow

Wallis et al. (56) studied counter-current annular flow in vertical tubes. Flow characteristics, such as air and water flow rates, pressure losses, pressure gradients, and liquid fraction, were investigated. Tube entry effects were also studied. A simple theory modeling the counter-current flow was developed.

Considering counter-current flow model shown in Fig. 2d, assuming incompressible and steady flow, a force balance for the gas core yields:

$$\frac{dP_g}{dz} + \rho_g z + \frac{4\tau_i}{D\alpha^{\frac{1}{2}}} = 0 \qquad (44)$$

where α is the void fraction, $(1-2\delta/D)^2$, δ the mean film thickness, D the tube ID and τ_i the interfacial shear stress.

Since the nominal gas velocity V_g is much larger than that of liquid V_f, the interface may be assumed to be stationary, and an interfacial friction factor can be defined as

$$f_i = \frac{2\tau_i \alpha^2}{\rho_g j_g}$$

where $j_g = 4Q_g/\pi D^2$ the mean volumetric gas flux.

For most cases, $(dP/dz) >> \rho_g g$, then

$$f_i = \frac{-(dP/dz)\ D\alpha^{5/2}}{2\rho_g j_g^2}$$

or

$$f_i = \frac{-(dP/dz)^*\ \alpha^{5/2}}{2j_g^{*2}}$$

where $(dP/dz)^* = (dP/dz)/[(\rho_f - \rho_g)g]$ and $j_g^* = \rho_g^{\frac{1}{2}} j_g/[(\rho_f - \rho_g)gD]^{\frac{1}{2}}$.

Additional force balance for the entire cross section of the tube gives:

$$\frac{dP_g}{dz} + P_g g + (1 - \alpha)(\rho_f - \rho_g)g = \frac{4\tau_w}{D} \tag{45}$$

where τ_w is the wall shear stress. A wall friction factor can be defined as

$$f_w = \frac{2\tau_w(1 - \alpha)^2}{\rho_f j_f^2}$$

where j_f is the mean volumetric liquid flux. Combining Eq. (44) and (45) yields a relation for gas and liquid flow rate as

$$\frac{2f_i j_g^{*2}}{\alpha^{5/2}} + \frac{2f_w j_f^{*2}}{(1-\alpha)^2} = (1 - \alpha) \tag{46}$$

With known f_i and f_w (from experiments), the limiting j_f^* and j_g^* can be obtained as an envelope of curves generated by Eq. (46) with $(1-\alpha)$ as a parameter. This corresponds to the "theoretical" maximum which may be obtained if entry effects can be minimized. Experimental results showed that smoother entry geometry yielded higher limiting gas and liquid flux (8,16,24).

Air-water counter-current flow experiments were conducted in 2.5 and 5.1 cm ID (1 and 2 in.) tubes. Wallis et al. suggested that there are three possible flow regions in counter-current annular flows. Region A where the wall shear stress

is dominant, Region B where the interfacial shear stress is dominant, and Region C where both A and B occur simultaneously within the tube. Tube entry geometries were found to strongly influence the transitions from Region A to Region B. Interfacial friction factors for 2.5 and 5.1 cm ID tubes were deduced from experimental data to be

$$f_i = 0.005 + 14.6\ (1 - \alpha)^n \qquad (47)$$

where n = 2.13 for 2.5 cm ID and 1.87 for 5.1 cm ID. The wall friction factor f_w is assumed to be 0.005.

With the above two friction factor values, Eq. (46) was used to solve the liquid fraction $(1-\alpha)$ and pressure gradient variations with gas flux. These results compared well with the measurements.

5.0 REFERENCES

1. T. K. Sherwood, G. H. Shipley and F. A. L. Holloway, Flooding Velocities in Packed Columns, Ind. Eng. Chem., 30, 765 (1938).

2. W. E. Lobo, L. Friend, F. Hashmall and F. Zenz, Limiting Capacity of Dumped Tower Packings, Trans. AIChE, 41, 693 (1945).

3. G. B. Wallis, One-Dimensional Two-Phase Flows, McGraw-Hill Book Company, New York (1969).

4. G. F. Hewitt and N. S. Hall-Taylor, Annular Two-Phase Flow, Pergmon Press, Oxford (1970).

5. J. A. Block and V. E. Schrock, Emergency Cooling Water Delivery to the Core Inlet of PWR's During LOCA, ASME Sym. on the Thermal and Hydraulic Aspects of Nuclear Reactor Safety, 1, 109 (1977).

6. R. T. Lahey, The Status of Boiling Water Nuclear Reactor Safety Technology, ASME Sym. on the Thermal and Hydraulic Aspects of Nuclear Reactor Safety, 1, 151 (1977).

7. S. Suzuki and T. Ueda, Behavior of Liquid Films and Flooding in Counter-Current Two-Phase Flows - Part 1, Flow in Circular Tubes, Int. J. of Multiphase Flow, 3, 517 (1977).

8. G. B. Wallis, Flooding Velocities for Air and Water in Vertical Tubes, UKAEA Report AEEW-R123 (1961).

9. T. W. Lovell, The Effect of Scale on Two-Phase Counter-Current Flow Flooding in Vertical Tubes, M.S. Thesis, Dartmouth College (1977).

10. O. L. Pushkina and Y. L. Sorokin, Breakdown of Liquid Film Motion in Vertical Tubes, Heat Transfer-Soviet Research, 1, 56 (1969).

11. A. E. Dukler and L. Smith, Two-Phase Interactions in Counter-Current Flow Studies of the Flooding Mechanism, NUREG-0214 (1977).

12. G. B. Wallis, C. J. Crowley and J. Block, ECC Bypass Studies, Paper presented at the AIChE Symposium on Light Water Reactor Safety, Boston, MA (1975).

13. C. J. Shearer and J. F. Davidson, The Investigation of a Standing Wave Due to Gas Blowing Upwards Over a Liquid Film - Its Relation to Flooding in Wetted Wall Columns, J. Fluid Mech., 22, 321 (1965).

14. A. G. Cetinbudaklar and G. J. Jameson, The Mechanism of Flooding in Vertical Counter-Current Two-Phase Flow, Chem. Eng. Sci., 24, 1669 (1969).

15. H. Imura, H. Kusuda and S. Funatsu, Flooding Velocity in a Counter-Current Annular Two-Phase Flow, Chem. Eng. Sci., 32, 78 (1977).

16. K. S. Chung, Flooding Phenomena in Counter-Current Two-Phase Flow Systems, Ph.D. Thesis, University of California, Berkeley (1978).

17. M. A. Grolmes, G. A. Lambert and H. K. Fauske, Flooding in Vertical Tubes, AIChE Symposium on Multiphase Flow Systems, Paper No. 38 (1974).

18. N. Y. Tobilevich, I. I. Sagan' and Y. G. Porzhezihskii, The Downward Motion of a Liquid Film in Vertical Tubes in an Air-Vapor Counter Flow, J. of Eng. Phys., 15, 1071 (1968).

19. G. B. Wallis and J. T. Kuo, The Behavior of Gas-Liquid Interfaces in Vertical Tubes, Int. J. of Multiphase Flow, 2, 521 (1976).

20. S. G. Bankoff, Entrapment of Gas in the Spreading of a Liquid over a Rough Surface, AIChE Journal, 4, 24 (1958).

21. T. Ueda and S. Suzuki, Behavior of Liquid Films and Flooding in Counter-Current Two-Phase Flow, Part 2, Flow in Annuli and Rod Bundles, Int. J. of Multiphase Flow, 4, 157 (1978).

22. S. Ostrach and A. Koestel, Film Instabilities in Two-Phase Flows, AIChE Journal, 11, 294 (1965).

23. D. J. Nicklin and J. F. Davidson, The Onset of Instability in Two-Phase Slug Flow, Two-Phase Fluid Flow Symposium, I. Mech. E., Paper No. 4 (1962).

24. G. F. Hewitt and G. B. Wallis, Flooding and Associated Phenomena in Falling Film Flow in a Vertical Tube, Winter Annual Meeting of ASME, 62 (1963).

25. R. Clift, C. L. Pritchar and R. M. Nedderman, The Effect of Viscosity on the Flooding Conditions in Wetted Wall Columns, Chem. Eng. Sci., 21, 87 (1966).

26. L. O. Jones and S. Whitaker, An Experimental Study of Falling Liquid Films, AIChE Journal, 12 (1966).

27. S. S. Kutateladze, Elements of the Hychodynamics of Gas-Liquid Systems, Fluid Mechanics - Soviet Research, 1, 29 (1972).

28. Y. Y. Hsu and R. W. Graham, Transport Processes in Boiling and Two-Phase Systems, McGraw-Hill Book Company, New York (1976).

29. S. Kamei, J. Oishi and T. Okane, Flooding in a Wetted Wall Tower, Chem. Eng. (Jap.), 18, 364 (1954).

30. K. Feind, Falling Liquid Films with Countercurrent Air Flow in Vertical Tubes, VDI - Forschungsheft 481, 26, 5 (1960)

31. J. A. Block and G. B. Wallis, Heat Transfer and Fluid Flows Limited by Flooding, AIChE Paper No. 20, 15th National Heat Trasf. Conf. (1975).

32. G. B. Wallis, The Influence of Liquid Viscosity on Flooding in a Vertical Tube, G.E. Report No. 62 GL132 (1962).

33. K. G. English, W. T. Jones, R. C. Spillers and V. Orr, Flooding in a Vertical Updraft Partial Condenser, Chem. Eng. Prog., 59, 51 (1963).

34. G. B. Wallis and S. Makkenchery, The Hanging Film Phenomenon in Vertical Annular Two-Phase Flow, J. of Fluids Eng., 96, 297 (1974).

35. J. E. Diehl and C. R. Koppany, Flooding Velocity Correlation for Gas-Liquid Counter Flow in Vertical Tubes, Chem. Eng. Prog. Symp. Series, 65, 77 (1969).

36. G. F. Hewitt, Influence of End Conditions, Tube Inclination and Physical Properties on Flooding in Gas-Liquid Flows, Private Communication (1977).

37. V. P. Alekseev, A. E. Poberezkin and P. V. Germsimov, Determination of Flooding Rates in Regular Packings, Heat Transfer-Soviet Research, 4, 159 (1972).

38. R. K. Sakhuja, Flooding Constraint in Wickless Heat Pipes, ASME paper 73-WA/HT-7 (1973).

39. Y. Hagi, Air-Water Flooding for Parallel Channel Flows Based on the Results for Single Path Flows, M.S. Thesis, Dartmouth College (1976).

40. G. F. Hewitt, P. M. C. Lacey and B. Nicholls, Transitions in Film Flow on a Vertical Tube, AERE-R4614 (1965).

41. G. L. Shires and A. R. Pickering, The Flooding Phenomenon in Counter-Current Two-Phase Flow, Sym. on Two-Phase Flow Proceedings, Exeter, 2, B501 (1966).

42. C. L. Tien, A Simple Analytical Model for Counter-Current Flow Limiting Phenomena with Condensation, Letters in Heat Transfer and Mass Transfer, 4, 231 (1977).

43. J. A. Block and C. J. Crowley, Effect of Steam Upflow and Superheated Walls on ECC Delivery in a Simulated Multiloop PWR Geometry, Creare TN-210 (1975).

44. D. D. Jones, Subcooled Counter-Current Flow Limiting Characteristics of the Upper Region of a BWR Fuel Bundle, NEDG-23549 (1977).

45. E. Elias and G. Yadigaroglu, Rewetting and Liquid Entrainment During Reflooding - State of the Art, EPRI NP-435 (1977).

46. C. Boyadjiev, D. Mitev and V. Beshkov, Laminar Boundary Layers at a Moving Interface Generated by Counter-Current Gas-Liquid Stratified Flow, Int. J. of Multiphase Flow, 3, 61 (1976).

47. S. A. Naff and J. F. Whitebeck, Steady State Investigation of Entrainment and Counter-Current Flow in Small Vessels, Topical Meeting on Water Reactor Safety, Conference Paper F30304, 212 (1973).

48. D. J. Hanson, C. E. Cantmill, K. R. Perkins, C. J. Shaffer and D. M. Snider, ECC Performance in the Semiscale Geometry, Aerojet Report ANCR-1161 (1974).

49. C. J. Crowley, G. B. Wallis and D. L. Ludwig, Steam/Water Interaction in a Scaled Pressurized Water Reactor Downcomer Annulus, COO-2294-4, Dartmouth College (1974).

50. R. A. Cudnik and R. O. Wooton, Penetration of Injected ECC Water Through the Downcomer Annulus in the Presence of Recovered Core Steam Flow, Battelle, Columbus (1974).

51. D. M. Speyer and L. Kmetyk, Flooding in Multichannel Two-Phase Counter-Flow, in Nuclear Reactor Safety Heat Transfer, 55-62, ASME, New York (1977).

52. R. J. Tobin, CCFL Test Results - Phase 1 - TLTA 7x7 Bundle, G.E. BWR/ECC Program, 7th Monthly Report (1977).

53. K. H. Sun and R. T. Fernandez, Counter-Current Flow Limitation Correlation for BWR Bundles during LOCA, ANS Transactions, 27, 625 (1977).

54. C. M. Mohr and J. K. Jacoby, Quick Look Report on KUU Support Column Air-Water Experiment (Series G2), EG & G Report RDW-23-78 (1978).

55. C. M. Mohr and D. A. Lopez, Quick Look Report on Supplemental Air-Water Upper Plenum Tests, EG & G Report RDW-47-78 (1978).

56. G. B. Wallis, H. J. Richter and D. Bharathan, Air-Water Counter-Current Annular Flow in Vertical Tubes, EPRI NP-786 (1978).

Table 1 SUMMARY OF VARIOUS EXPERIMENTS AND CORRELATIONS FOR SINGLE TUBE GEOMETRY

AUTHOR	TUBE GEOMETRY Liq. Inlet Liq. Exit	FLUIDS TESTED	TUBE DIAMETER $X10^{-2}$m (in)	FLOODING CORRELATION	COMMENTS
Kami et al. (29)		air-water air-millet jelly solution air-soap solution	0.19, 0.32, 0.42, 0.49 (0.75, 1.25, 1.65, 1.93)	$\frac{\rho_g j_g}{\rho_f j_f} = 198\ (\frac{4\rho_f j_f}{\pi D \mu_f})^{-1.225} (\frac{\sigma}{D^2 \rho_f g})^{-0.23} (\frac{\mu_g}{\mu_f})^{0.71} (\frac{\rho_g}{\rho_f})^{0.13} (\frac{D^3 \rho_f^2 g}{\mu_f})^{0.231}$	
Feind (30)	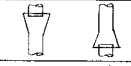		2.0, 5.0 (0.79, 1.97)	$M(\frac{Re_g}{Re_f^n})(\frac{\rho_g}{\rho_f})^{2/5} (\frac{\mu_g}{\mu_f})^{3/4} + 1.4 \times 10^4 = 1300\ (\frac{R}{\delta})^{5/4}$ for $Re_f \leq 400$, m = 53.2, n = 1/3 for $Re_f > 400$, m = 157.7, n = 1/2	
Wallis (8)	1.  2. 3.	air-water	1.27, 1.91, 2.54, 5.1, (1/2, 3/4, 1, 2)	$j_g^{*1/2} + j_f^{*1/2} = c$ where $j_i^* = j_i \rho_i^{1/2} [Dg(\rho_f - \rho_g)]^{-1/2}$ $i = g,f$ and $0.725 \leq c \leq 0.875$	1. Tube diameter and entry geometry were found to be important. 2. C takes on larger value for smoother entry.
Hewitt and Wallis (24)	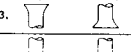	air-water	3.18 (1-1/4)	$j_g^{*1/2} + j_f^{*1/2} = 1$	For porous liquid injection and removal, c is nearly unity.
English et al. (33)	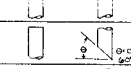	steam-water	1.91 (3/4)	$\rho_g j_g = \frac{1550 D^{0.3} \rho_f^{0.46} \rho_g^{0.5} \sigma^{0.9}}{\mu_f^{0.14} (\cos\theta)^{0.32} (\rho_f j_f / \rho_g j_g)^{0.07}}$	The tube end cutting has positive effect on flooding velocities
Clift et al. (25)	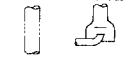	air-water air-glycerol (25%, 59%, 70%, 77% & 82%)	3.18 (1-1/4)	$j_g^{*1/2} + 0.34\ j_f^{*1/2} = 0.79$ (for air-water)	Flooding velocities decrease with higher viscosity.
Tobilevich et al. (18)	Evaporator	air-water steam-water air-sugar solution	3.27, 5.25, 3.0 (1.29, 2.07, 1.18)	$Fr = a \exp\{bK (\rho_g/\rho_f)^{0.2}\}$ for Fr > 0.012, a = 1.29, b = -14.14 for Fr < 0.012, a = 0.0653, b = -10.12	The use of sugar solution did not reveal the viscosity effect since density of sugar solution is considerably different from that of water.
Pushkina and Sorokin (10)	1.  2.	air-water	for geometry 1: 30.9 (12.17) for geometry 2: 0.62 0.88, 0.9, 1.22 (0.24, 0.35, 0.48)	$K_{cr} = 3.2$ where $K = j_g \rho_g^{1/2} [g\sigma(\rho_f - \rho_g)]^{-1/4}$	The critical Kutateladze number is independent of the hydraulic diameter.

Table 1 SUMMARY OF VARIOUS EXPERIMENTS AND CORRELATIONS FOR SINGLE TUBE GEOMETRY .....(continued)

AUTHOR	TUBE GEOMETRY Liq. Inlet	Liq. Exit	FLUIDS TESTED	TUBE DIAMETER $X10^{-2}$m (in)	FLOODING CORRELATION	COMMENTS
Diehl and Koppany (35)					$j_g = a\{f_1 f_2 (\sigma/\rho_g)^{1/2}\}^b$	
Alekeev et al. (37)					$K_{cr} = 3.2\ Fr^{-0.22} We^{-0.26}$ where $Fr = Q_f(\rho_f - \rho_g)^{3/4} g^{-1/2} \sigma^{-3/4}$ and $We = \sigma/(\rho_f - \rho_g) g D_{eq}^{\ 3}$	The flooding data were collected from various experiments.
Grolmes et al. (17)			nitrogen-water	0.4, 0.6, 1.3, 2.5 (0.16, 0.24, 0.51, 0.99)	$j_g = 1.15 \left(\frac{\rho_f}{\rho_g} \frac{g\delta}{0.006 + \frac{200\delta^2}{(\nu/\nu_R)^{0.44}}}\right)^{1/2}$	1. A large L/D ratio was tested. 2. Little effect was observed for tube diameter and L/D ratio.
Dukler et al. (11)	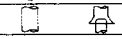		air-water	5.1 (2)	$j_g^{*1/2} + j_f^{*1/2} = 0.88$	The constant c value is the same as that obtained by Wallis for nozzle entry (8).
Hewitt (36)	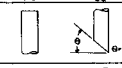		air-water air-silicon oil air-glycerol (38% & 67%)	1.27, 3.18 (1/2, 1-1/4)	$j_g^{*1/2} + j_f^{*1/2} = c$	1. Two different tube lengths were used: 1.22 and 2.44 m (4 and 8 ft; little length effect was observed 2. Tube diameter and tube end cutting effect flooding velocities. 3. Viscosity is stabilizing, but surface tension is unstablizing. 4. Flooding velocities increase for small tube inclination.
Imura et al. (15)			air-water air-ethynol air-ethylene glycol air-n neptane	1.12, 1.60, 2.10, 2.42 (0.44, 0.63, 0.83, 0.95)	$\frac{G}{L}\left(1 + \frac{G}{L}\frac{\rho_g}{\rho_f}\frac{S_g}{S_f}\right) = \frac{S_g}{S}\frac{1}{L}\left(\frac{\rho_g \sigma}{\delta}\right)\left(\zeta - \left(\frac{1}{R/\delta - 1}\right)^{1/2}\right)^{1/2}$	For actual values of G, L, S_g, S, ζ and δ, refer Eq. (31).
Suzuki and Ueda (7)			air-water air-glycerol air-sec.-octynol	1.0, 1.8, 2.88 (0.39, 0.71, 1.13)	$Fr = A\log_{10} X + B$	1. For actual values of A, X and B, refer Eq. (32). 2. Tube diameter and length were found to be important. 3. Viscosity is stabilizing, but surface tension showed no definite trend
Chung (16)	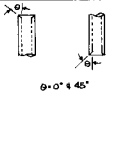		air-water		$K_g^{1/2} + K_f^{1/2} = C_K$ where $C_K \simeq 2$ for $\theta = 45°$ entry	1. Tube entry condition is an important factor 2. There is no observable trend for tube diameter effect.

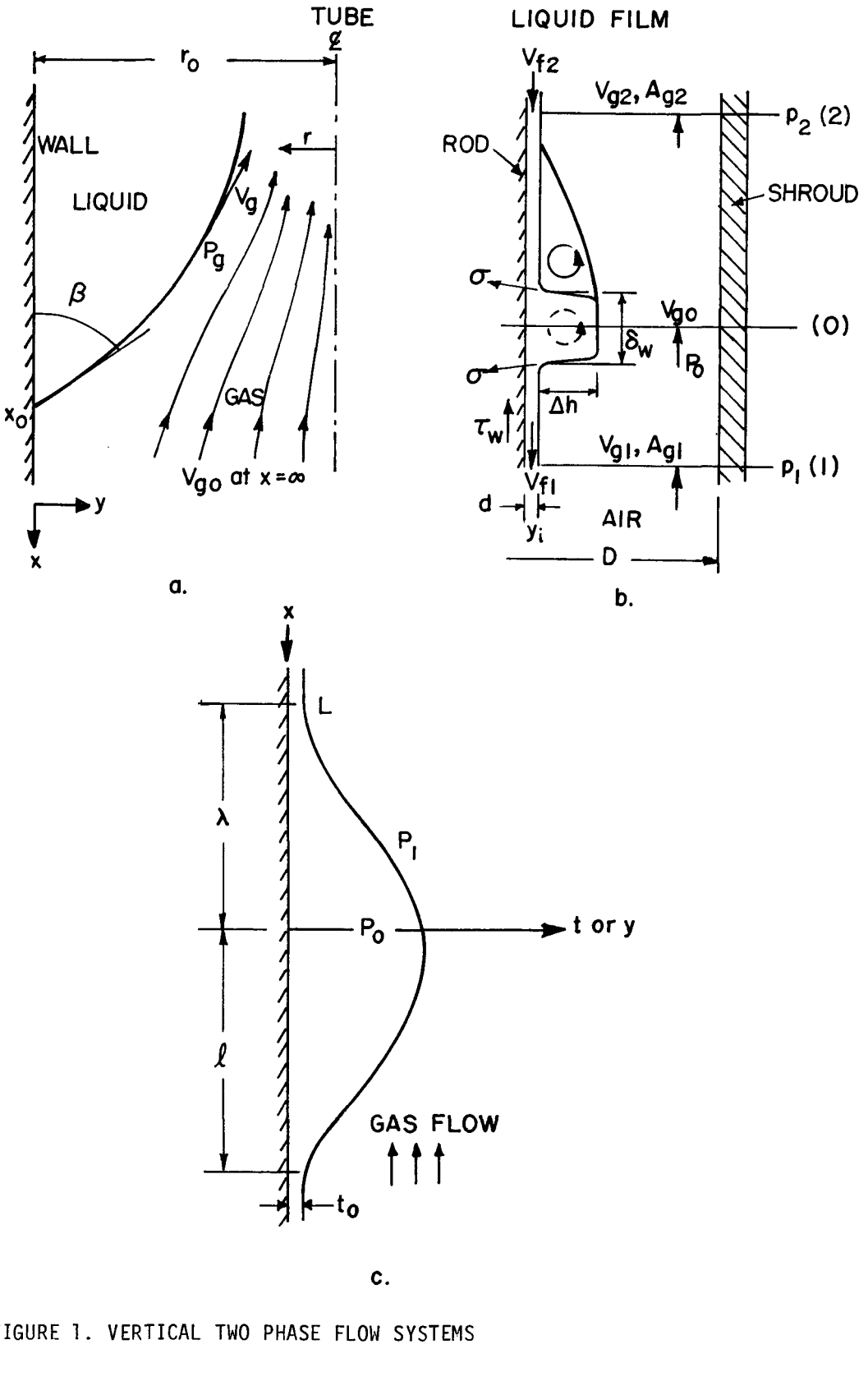

FIGURE 1. VERTICAL TWO PHASE FLOW SYSTEMS

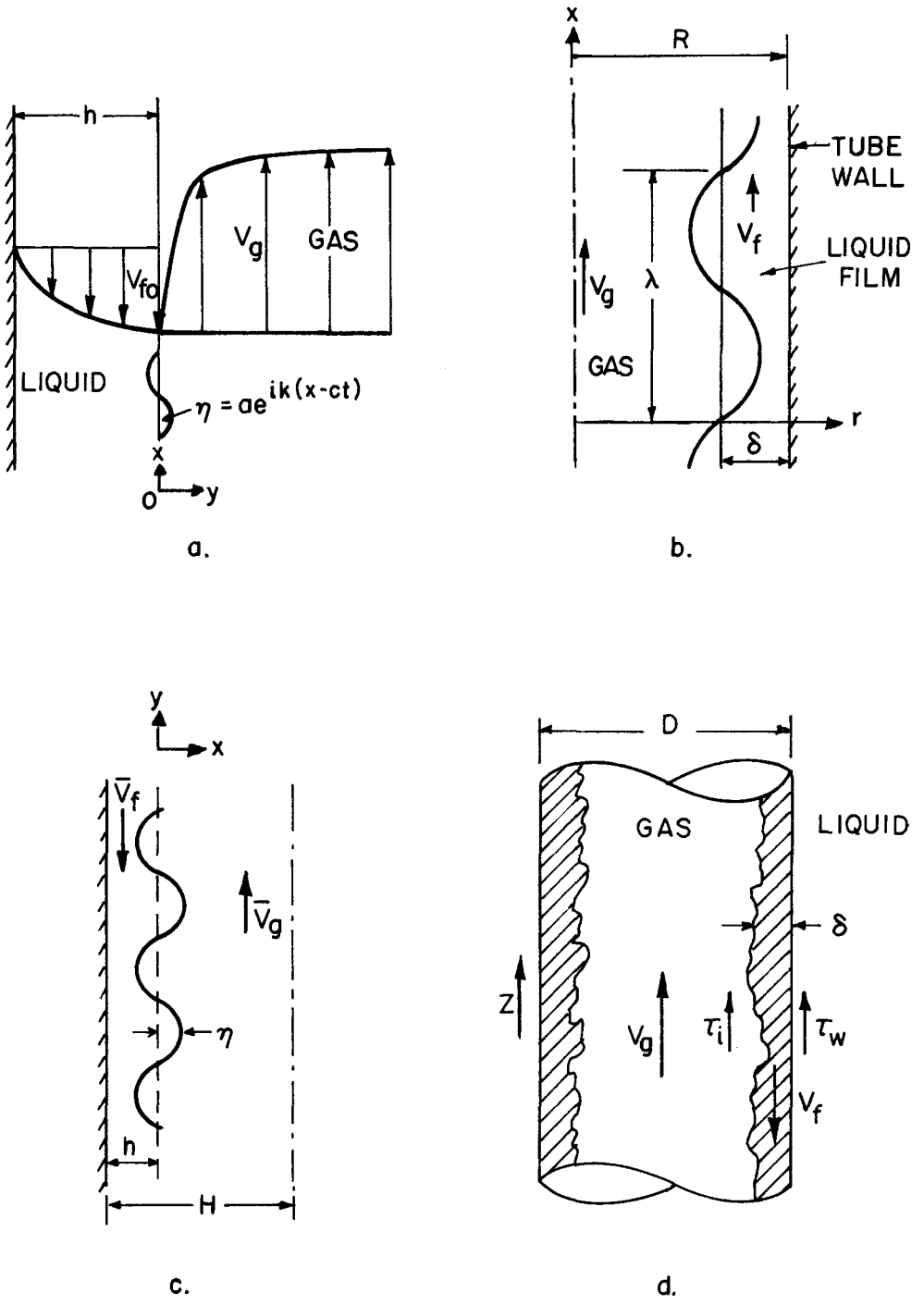

FIGURE 2. VERTICAL TWO PHASE FLOW SYSTEMS

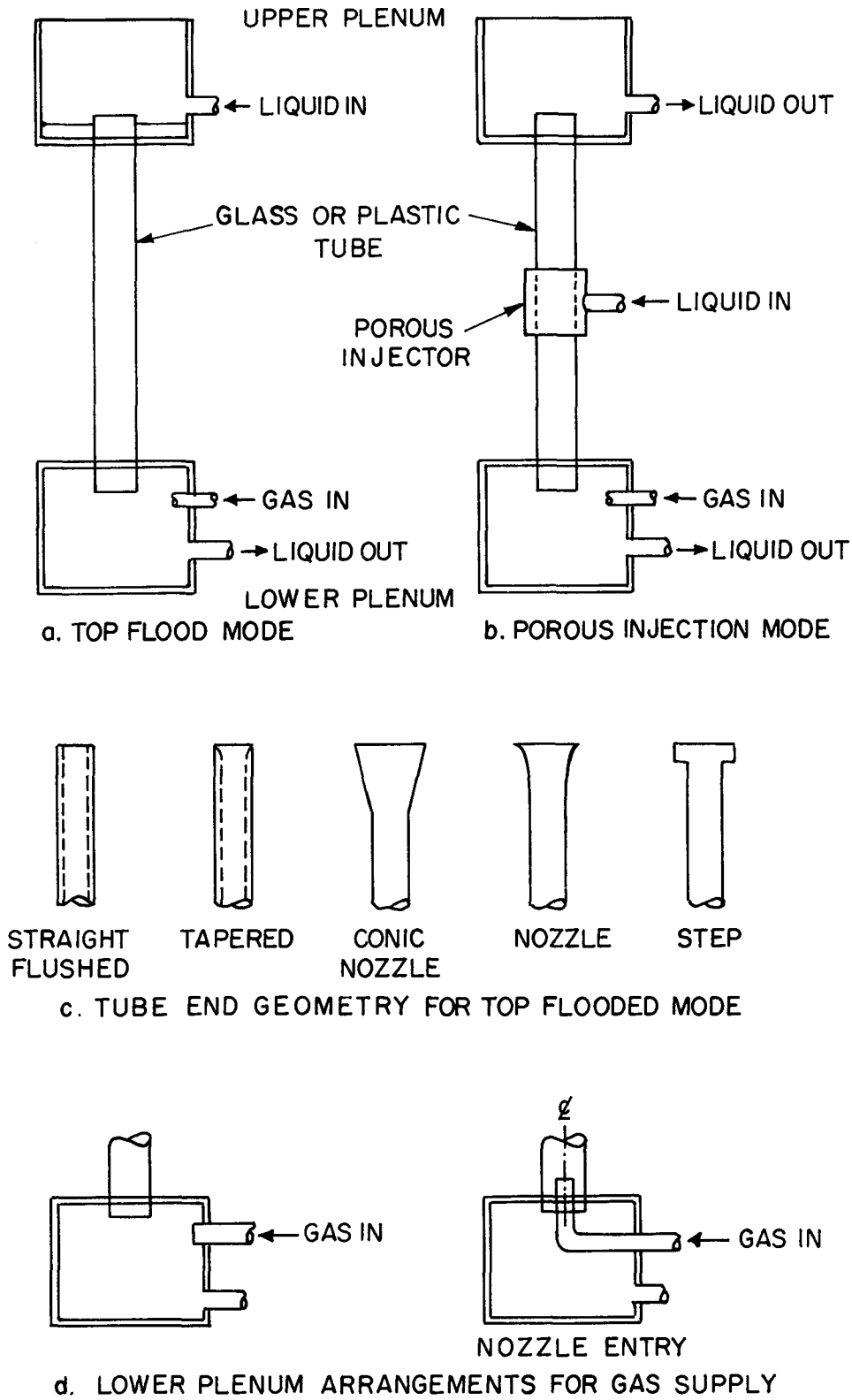

FIGURE 3. TYPICAL APPARATUS ARRANGEMENT FOR VERTICAL CHANNEL FLOODING EXPERIMENTS